On the Dependence of Sea Surface Roughness on Wind Waves

H. K. JOHNSON

Danish Hydraulic Institute, Hørsholm, Denmark

J. HØJSTRUP

Risø National Laboratory, Roskilde, Denmark

H. J. VESTED

Danish Hydraulic Institute, Hørsholm, Denmark

S. E. LARSEN

Risø National Laboratory, Roskilde, Denmark

(Manuscript received 8 November 1996, in final form 14 November 1997)

ABSTRACT

The influence of wind waves on the momentum transfer (wind stress) between the atmosphere and sea surface was studied using new measured data from the RASEX experiment and other datasets compiled by Donelan et al.

Results of the data analysis indicate that errors in wind friction velocity u_* of about $\pm 10\%$ make it difficult to conclude on the trend in z_{ch} using measured data from a particular dataset. This problem is solved by combining different field data together. This gives a trend of decreasing z_{ch} with wave age, expressed as: $z_{ch} = 1.89(c_p/u_*)^{-1.59}$.

Furthermore, it is shown that calculations of the wind friction velocities using the wave-spectra-dependent expression of Hansen and Larsen agrees quite well with measured values during RASEX. It also gives a trend in Charnock parameter consistent with that found by combining the field data. Last, calculations using a constant Charnock parameter (0.018) also give very good results for the wind friction velocities at the RASEX site.

1. Introduction

In the past 15 years, there has been an increasing interest in the description and measurement of the exchange of momentum at the air–sea interface. The motivation for these studies is that many important processes such as wind wave growth, storm surges, and atmospheric circulation are influenced by the exchange of momentum at the air–sea interface. This momentum exchange is determined to a large extent by the aerodynamic roughness at the air–sea interface since it is this roughness that determines the turbulence level near the air–sea interface, and thus the wind stress.

Generally, many experimental studies have shown that there is a relationship between the roughness at the air–sea interface and the wave climate (e.g., Merzi and Graf 1985; Geernaert et al. 1987; Toba et al. 1990; Smith et al. 1992; Donelan et al. 1993). However, the form of this relationship is not quite settled, partly because of the different observed behavior between field and laboratory waves, and partly also because of the scatter in the data. Further experimental studies are being carried out in an attempt to clarify this relationship. RASEX (Risø Air–Sea Exchange) is one such experiment designed, among other objectives, to investigate the exchange of momentum at the air–sea interface (Barthelmie et al. 1994). Compared with other similar experiments, RASEX is characterized by being located in rather shallow waters (depths of about 3 to 4 m near the measurement site) in an area where the waves are predominantly fetch limited. In this paper, a selected subset of this data (based on a detailed dimensionless analysis of the problem) is used to investigate the dependence of the sea roughness on wave parameters.

Furthermore, we also investigate the use of a recently developed model of sea roughness (Hansen and Larsen 1997) for calculating wind friction velocities.

The plan of this paper is as follows: In section 2, we

Corresponding author address: Dr. H. K. Johnson, Dr. Nik & Associates, 20-2, Jalan Setiawangsa 10, Taman Setiawangsa 54200 Kuala Lumpur.
E-mail: hkj@pd.jaring.my

present the existing evidence from the literature on the relationship between the sea roughness and waves; this is followed by a brief description of the instrumentation for the RASEX field campaign in section 3. Section 4 follows with a dimensionless analysis of the air–sea interaction problem, leading to an analysis of the RASEX data and a suggested relationship between sea roughness and wave age. The application of the Hansen and Larsen model is discussed in section 5, followed by a summary of the work done and the conclusions in section 6.

2. Evidence from literature

In the last 15 years, several experiments have been carried out to investigate the dependence of sea roughness and/or the aerodynamic drag on wave parameters. In many of these experiments, attempts were made to relate the dimensionless sea roughness, gz_0/u_*^2 (widely known as the Charnock parameter) to wave age (c_p/u_* or c_p/U_{10}). Results from some of these experiments are described in the following paragraphs.

Donelan (1982) carried out measurements of wind stress using the eddy correlation technique and wave parameters in Lake Ontario at a water depth of 12 m. He found that the Charnock parameter, z_{ch}, generally increases with decreasing wave age (c_p/U_{10}), although with a lot of scatter in the data.

Merzi and Graf (1985) carried out wind and wave measurements in water depth of 3 m in the lake of Geneva. They measured wind stress using the profile method and found (with a lot of scatter) that the dimensionless sea roughness z_0/H_{m0} increases with decreasing wave age (c_p/u_*).

Geernaert et al. (1987) carried out measurements on a North Sea platform in a water depth of 30 m in the German Bight. They measured wind stress using the eddy correlation technique and estimated waves from fetch scaling relations. They found that the estimated drag coefficient from their dataset decreases with increasing wave age (c_p/u_*). This behavior was found to be consistent with the MARSEN dataset (consisting of measured wind stress and waves) analyzed in Geernaert et al. (1986).

Maat et al. (1991) and Smith et al. (1992) analyzed measurements of wind stress and waves collected during the HEXOS experiment near a platform 9 km off the Dutch coast in a water depth of 18 m. They concluded from these measurements that the Charnock parameter decreases with increasing wave age.

Toba et al. (1990) measured wind speed, wave height, and period from an oil platform in the Bass Strait, Australia. Considering only waves in local equilibrium with the wind, they used the 3/2 power law to infer the wind stress estimates. They analyzed this data together with other data from tower stations and laboratory experiments, and concluded that the Charnock parameter increases with increasing wave age (c_p/u_*). This result is significantly different from other results mentioned above. Toba et al. suggested that the difference between their results and that of Geernaert et al. (1987) may be due to the inclusion of swell wave conditions in the data by Geernaert et al., which are not in equilibrium with the local wind.

Donelan (1990) and Donelan et al. (1993) analyzed a composite dataset of waves and wind stress from the field (Lake Ontario, HEXOS, and from an exposed site in the Atlantic Ocean off the coast of Nova Scotia) and for the laboratory [Donelan (1990) wave tank and Keller et al. (1992) wave tank] separately. They found that younger waves in the field are generally rougher than mature waves, while this is not necessarily the case for the laboratory data. Thus, the Charnock parameter (for the field data) decreases with increasing wave (c_p/u_*). They argued that laboratory waves should not be analyzed together with field data, as was done by Toba et al. (1990), since the laboratory waves are much smoother than their field equivalents and consequently behave in a different way than field waves.

From the preceding paragraphs, it appears there is evidence from measurements that the dimensionless sea roughness (or Charnock parameter) depends on the wave age. The form of this relationship is, however, not settled.

One reason for this discrepancy is differences in the type of data selected for analysis. For instance, while some authors analyze data with only locally generated wind waves in equilibrium with the local wind, others include cases with swell waves in the analysis. Also, it is not clear if some investigators included data for smooth flows in the analysis since some did not state explicitly that only rough flows were included in their analysis. It is shown later in this paper (section 4) that the dimensionless sea roughness depends on wave age alone only for particular conditions. Hence, in cases where these conditions are not met, other parameters should be included in the analysis. In addition, some investigators used a mixture of measured and calculated quantities in order to determine the relationship between wind stress and waves, and this may have conditioned the observed behavior somewhat. A review of problems associated with the parameterization of momentum fluxes over sea waves is presented in Komen et al. (1996, submitted to *J. Global Atmos. Ocean Syst.*).

Aside from the problem with selected datasets, an error estimate for the Charnock parameter (corresponding to the errors in measured wind stress) is not usually given. The absence of error estimates make it difficult to conclude whether the observed trend is larger than the scatter or vice versa. This is especially so in this case where the scatter in the data is usually large. This problem is addressed in section 4 of this paper.

3. The RASEX field campaigns

The data in this paper originate from the RASEX measurements, which took place at an offshore wind

turbine site in Denmark in a spring and a fall campaign in 1994. The experiment comprises two 48 m offshore towers and one tower on the coast on the island of Lolland. The tower used for this study was situated in about 4-m water depth with an upstream fetch of 15–20 km in a 90 degree sector with upstream water depths of 5–20 m (see Fig. 1).

For this paper, we used the lowest sonic anemometer (Solent, 3-component research type) mounted 3 m above MSL. Data were logged as 30-min time series sampled at 20 Hz, which were subsequently subjected to a coordinate transformation to orient the x-axis into the mean wind. A linear trend was removed from the data before the covariances were calculated. The estimated uncertainty on the resulting value of u_* is about 10%.

The mean wind speed was derived from the lowest cup anemometer at 7 m, measuring mean wind speed with an estimated accuracy of about 2%.

The wave gauge was an acoustic device placed on the sea bottom about 30 m west-northwest from the tower, measuring the water level fluctuations eight times per second. Again 30-min time series were logged, and power spectra were calculated by use of FFT. From the spectra three frequencies, f_{25}, f_{50}, and f_{75}, were derived at 25%, 50%, and 75% accumulated variances. Then f_{50} was used as a measure of the peak frequency of the spectrum, and BW $= \log_{10}(f_{75}/f_{25})$ then serves as a measure of the widths of the spectral peaks. Rather than computing the peak frequency directly, we chose the statistically more stable way of computing f_{50}, which means that we need to assume a model for the spectra to arrive at the correct peak frequency. A JONSWAP model (see section 5) fits the data well with a peak enhancement factor of 1.0 (in the JONSWAP experiment, the mean value for this parameter was found to be 3.3).

The dataset

There were available 1987 30-min time series from the RASEX experiments, taken at the Vindeby site during spring and fall 1994. From the time series a number of characteristic parameters were computed. The data were sampled at 8 Hz, but a cutoff frequency of 2 Hz was applied to minimize the influence of noise.

The available data are:

T_{50}: Period of spectrum computed such that 50% of the variance in the spectrum is found on either side of the frequency $1/T_{50}$. This frequency is slightly larger than the actual peak frequency in our model spectrum. The peak frequency corresponding to the fitted JONSWAP spectrum is computed as $f_p = 1/(1.156T_{50})$.

T_m: Mean period of waves $= m_0/m_1$, where m_i is the spectral moment: $m_i = \int_{-\infty}^{\infty} f^i S(f)\, df$.

T_z: Wave period based on zero crossing frequency $= (m_0/m_2)^{0.5}$.

H_s: Significant wave height derived as four times the standard deviation of the surface elevations.

BW: The bandwidth of the spectrum, defined as BW $= \log_{10}(f_{75}/f_{25})$, where f_{25} is the frequency at which the integrated variance is 25% of the total variance and f_{75} is the frequency at which the integrated variance is 75%. In other words, 50% of the variance is situated between the two frequencies. This parameter enables us to distinguish between data with two-peaked spectra (very wide) from the single peak spectra that are similar to our model (which has a BW of 0.171).

MSL: Water depth to mean sea level (m).

U_7: Average wind speed (m s^{-1}) at an elevation of 7 m above MSL.

U_{15}: Average wind speed (m s^{-1}) at an elevation of 15 m.

dir_{20}: Average wind direction (°N) at an elevation of 20 m.

u_*^2: Total wind stress (m s^{-1})^2 = sqrt($\langle uw\rangle^2 + \langle \theta w\rangle^2$), where $-\langle uw\rangle$ is the alongwind stress and $\langle \theta w\rangle$ is the stress perpendicular to mean wind.

4. Analysis of RASEX data

In this section we present results of the analysis of selected data collected during RASEX. First, we carry out a dimensionless analysis of the problem, next the measured and derived quantities are presented together with an assessment of errors, then the influence of wave age on sea roughness is examined, and finally some inferences are made from the data.

a. Dimensionless analysis

Any property, A, depending on the interaction between the air and the sea surface can be described generally as

$$A = f(\text{wind flow near sea, sea surface}). \quad (4.1)$$

The wind flow near the sea can be described in its most general form by the following independent parameters:

$$\text{wind} = f(u_*, \Phi_a, \rho_a, \mu_a, g, \theta_a, \text{sea surface}), \quad (4.2)$$

where u_* is the wind friction velocity, Φ_a is the wind direction, ρ_a is the density of air, μ_a is the dynamic viscosity of air, g is the acceleration due to gravity, and θ_a is the air temperature.

Similarly, the independent parameters describing the sea surface can be listed as

$$\text{sea surface} = f(H, T, \Phi_w, d, \rho_w, \mu_w, \theta_w, g, z_{0s}), \quad (4.3)$$

where H is a characteristic wave height (taken as H_{m0}—the significant wave height), T is a characteristic period (taken as T_p—the peak period), Φ_w is the wave direction, d is water depth, ρ_w is the density of water, μ_w is the dynamic viscosity of water, θ_w is the temperature of the

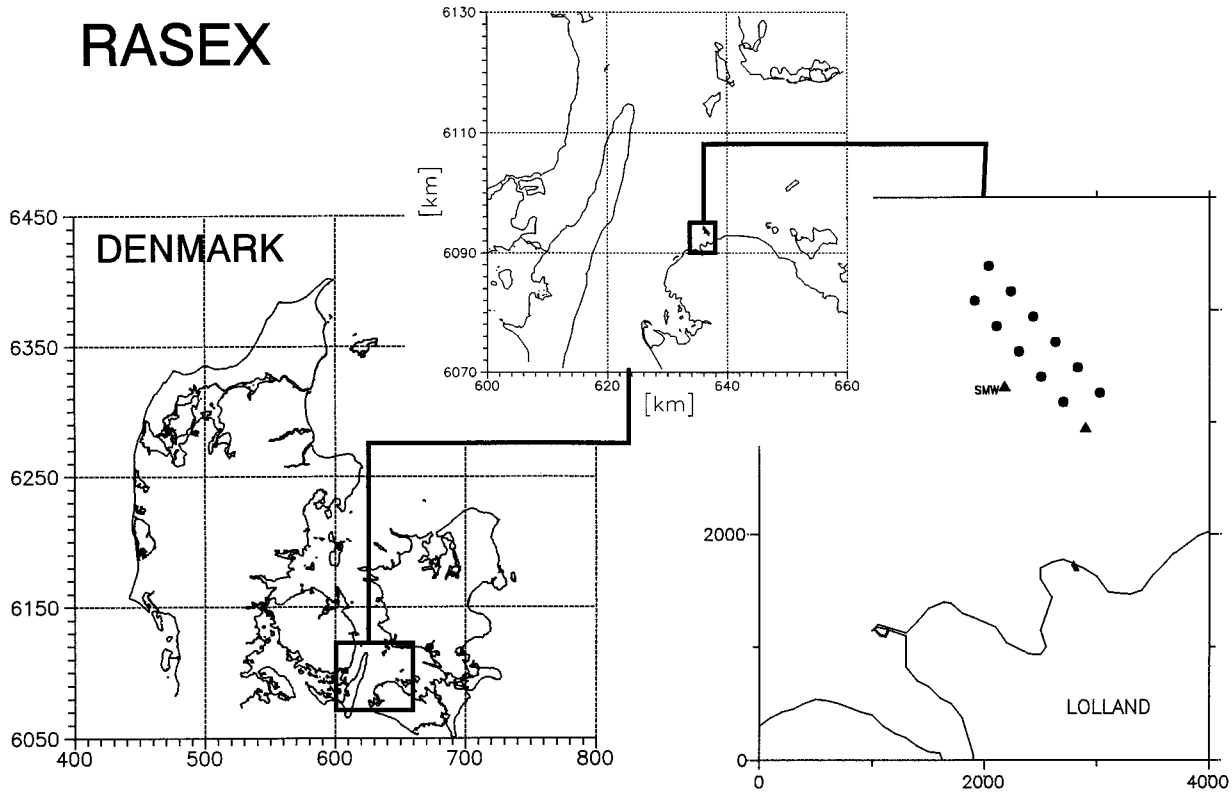

FIG. 1. The RASEX site at Vindeby. From left to right: Denmark–Langeland/Lolland–closeup of site. The filled circles are wind turbines, the triangles are the two 48-m offshore lattice towers and the coast tower. The tower used for this study was situated west of the wind farm (SMW). Distances on the two leftmost figures are in kilometers, on the closeup in meters.

water, g is the acceleration due to gravity, and z_{0s} is the background sea roughness (sea roughness in the absence of waves).

Thus, Eq. (4.1) can be rewritten as

$$A = f(u_*, \Phi_a, \rho_a, \nu_a, g, \theta_a, H_{m0}, T_p, \Phi_w, d, \rho_w, \nu_w, \theta_w, z_{0s}), \tag{4.4}$$

where μ has been replaced by the kinematic viscosity, $\nu = \mu/\rho$. Now, using ρ_a, g, and u_* as repeaters, the following dimensionless form of Eq. (4.4) can be obtained:

$$\tilde{A} = f\left(\Phi_a, \frac{u_*^3}{g\nu_a}, \theta, \frac{gH_{m0}}{u_*^2}, \frac{gT_p}{u_*}, \Phi_{wi}\frac{gd}{u_*^2}, \frac{\rho_w}{\rho_a}, \frac{u_*^3}{g\nu_w}, \theta_w, \frac{gz_{0s}}{U_*^2}\right)$$

or

$$\tilde{A} = f\left(\frac{gH_{m0}}{u_*^2}, \frac{gT_p}{u_*}, \frac{gd}{u_*^2}, \frac{gz_{0s}}{u_*^2}, \theta_a, \theta_w, \Phi_a, \Phi_w, \frac{u_*^3}{g\nu_a}, \frac{u_*^3}{g\nu_w}, \frac{\rho_w}{\rho_a}\right). \tag{4.5}$$

Now, we introduce a number of simplifications. First, we assume locally generated waves implying a relationship between H_{m0} and T_P (for instance, Toba's relationship), thus, we can drop one of H_{m0} and T_P. Next, we combine the second and third terms in the phase celerity c_p using the dispersion relationship. This assumes that the only influence of water depth is in the modification of the phase celerity. Obviously, this excludes situations where depth-induced breaking is important. Next we assume the sea surface is completely smooth in the absence of waves and drop the fourth term. Last we assume rough turbulent flow conditions at the air–sea interface (dropping the ninth and tenth terms). Now, Eq. (4.5) can be rewritten as

$$\tilde{A} = f\left(\frac{c_p}{u_*}, \theta_a, \theta_w, \Phi_a, \Phi_w, \rho_w/\rho_a\right). \tag{4.6}$$

In Eq (4.6) θ_a and θ_w contribute to the momentum exchange at the air–sea interface due to stratification, thus for neutrally stratified flows (in which case the air–sea temperature difference is small), they can be dropped from Eq. (4.6). Also, if we limit ourselves to cases where the wind and waves are nearly in the same direction, Φ_a and Φ_w can also be dropped from Eq. (4.6). Lastly, we consider situations with constant ρ_w/ρ_a, and drop this term. Hence Eq. (4.6) can be expressed as

$$\tilde{A} = f(c_p/u_*). \tag{4.7}$$

If $\tilde{A}$ is the dimensionless sea roughness at the air–sea interface, Eq. (4.7) can be written as

$$\frac{gz_0}{u_*^2} = f(c_p/u_*). \tag{4.8}$$

From the preceding paragraphs, Eq. (4.8) shows that the dimensionless sea roughness (or Charnock parameter) is a function of wave age only if the following conditions are satisfied: 1) locally generated wind waves, 2) rough turbulent flow conditions at the air–sea interface, 3) neutrally stratified conditions, 4) waves and wind in nearly the same direction, and 5) no background sea roughness (i.e., sea is smooth in the absence of waves).

b. Considerations for selecting a data subset for analysis

It is intended to investigate the dependence of the sea roughness on wave age. Based on the dimensionless analysis in the preceding section, a number of conditions must be satisfied in order for Eq. (4.8) to be valid. This therefore imposes the necessary considerations for selecting a data subset for analysis. These considerations are 1) locally generated waves, in which there is a definite relationship between H_{m0} and T_P; 2) rough turbulent flow conditions at the air–sea interface (following Toba et al. 1991), defined as cases with $u_* z_0/\nu > 2.3$); 3) neutrally stratified situations (or equivalent neutral parameters); and 4) wind and waves in nearly the same direction, which is assumed to be the case for locally generated waves with $\Phi_a = 270°\text{N} \pm 22.5°$.

c. Measured and derived quantities

In order to satisfy the third condition in section 4b, the measured winds were converted to equivalent neutral winds. In the presence of stratification, the wind profile can be written as in Eq. (4.9) following the Monin–Obukhov similarity theory:

$$U(z) = \frac{u_*}{\kappa}\left(\ln\frac{z}{z_0} - \Psi\right), \tag{4.9}$$

where Ψ is a stratification function. Now, defining the equivalent neutral wind, $U_n(z)$ as

$$U_n(z) = \frac{u_*}{\kappa}\ln\frac{z}{z_0}, \tag{4.10}$$

Eqs. (4.9) and (4.10) can be combined to give

$$U_n(z) = U(z) + \Psi u_*/\kappa. \tag{4.11}$$

Following Geernaert et al. (1988) the stratification function is given as

$$\Psi = \begin{cases} 2\ln\left(\dfrac{1+\Phi_m^{-1}}{2}\right) + \ln\left(\dfrac{1+\Phi_m^{-2}}{2}\right) - 2\tan^{-1}(\Phi_m^{-1}) + \pi/2, & z/L < 0 \quad (4.12a) \\ -5z/L, & z/L \geq 0, \quad (4.12b) \end{cases}$$

where $\Phi_m = (1 - 16z/L)^{-1/4}$ for $z/L < 0$; and L is the Monin–Obukhov length.

Thus, using the measured wind speed, wind friction velocity, and Monin–Obukhov length, the equivalent neutral wind speed at a given elevation is obtained. For this analysis, the neutral wind speed at 7-m elevation is corrected to 10-m elevation using the 1/7 power law. Thus

$$U_{10n} = U_{7n}\left(\frac{10}{7}\right)^{1/7}. \tag{4.13}$$

Given the neutral wind speed at 7-m elevation and the measured friction velocity, the sea roughness z_0, is calculated from Eq. (4.10). The neutral drag coefficient C_{dn} is calculated as

$$C_{dn} = u_*^2/U_{10n}^2, \tag{4.14}$$

while the phase speed at peak frequency c_p is calculated using the measured water depth and peak frequency in the linear dispersion relationship.

d. Data results

Table 1 presents the measured and derived data satisfying the conditions described in section 4b. A plot of the dimensionless wave energy $(1/16)(gH_{m0}/u_*^2)^2$ versus the dimensionless frequency $\omega_p u_*/g$ is shown in Fig. 2 for data runs satisfying the rough flow conditions ($u_* z_0/\nu > 2.3$) and winds from $270° \pm 22.5°$. The dotted line in Fig. 2 is the relationship suggested by Toba (1978). Figure 2 shows a unique relationship between H_{m0} and T_P, as assumed in section 4b.

Now, in order to investigate the functional form of Eq. (4.8), the Charnock parameter, $z_{\text{ch}}(=gz_0/u_*^2)$ is plotted against the inverse wave age (u_*/c_p) in Fig. 3. A weak trend of increasing z_{ch} with wave age can be observed. This trend is opposite to the widely believed trend of z_{ch} decreasing with wave age (Maat et al. 1991; Smith et al. 1992; Donelan 1990; Donelan et al. 1993). We note, however, that Toba et al. (1990) suggested the type of trend indicated in Fig. 3 (dashed line by Toba et al. 1990).

Before carrying out any further analysis, it is important to assess the potential errors in the z_{ch} derived from measurements. This is the subject of the section below.

e. Errors

Recall from Eq. (4.10) that the sea roughness z_0 is calculated as

$$z_0 = \frac{10}{\exp(\kappa U_{10n}/u_*)}. \tag{4.15}$$

Now, suppose there is an error in κ, U_{10n}, and u_*, given as $\Delta\kappa/\kappa$, $\Delta U_{10n}/U_{10n}$, $\Delta u_*/u_*$ respectively, then the corresponding error in z_0 ($\Delta z_0/z_0$) is given as

$$\frac{\Delta z_0}{z_0} + 1 = \exp\left\{\frac{-\kappa/\sqrt{C_{dn}}}{(1+\Delta u_*/u_*)} \times\left[\frac{\Delta U_{10n}}{U_{10n}} + \frac{\Delta\kappa}{\kappa} + \left(\frac{\Delta\kappa}{\kappa}\right)\left(\frac{\Delta U_{10n}}{U_{10n}}\right) - \frac{\Delta u_*}{u_*}\right]\right\}. \tag{4.16}$$

The corresponding error in the Charnock parameter ($\Delta z_{ch}/z_{ch}$) is given as

$$\frac{\Delta z_{ch}}{z_{ch}} + 1 = \frac{\Delta z_0/z_0 + 1}{(1 + \Delta u_*/u_*)^2}. \tag{4.17}$$

Lastly, the error in wave age can be written as

$$\frac{\Delta(c_p/u_*)}{c_p u_*} = \frac{\Delta c_p/c_p - \Delta u_*/u_*}{1 + \Delta u_*/u_*}. \tag{4.18}$$

Now, from section 3, the overall error in u_* is about $\pm 10\%$, while the error in U_{10} is generally much smaller, $<2\%$. Similarly, the errors in water depth, peak frequency, and thus phase celerity c_p, are small. Assuming κ equals 0.4 and C_{dn} is 1.5×10^{-3} (approximate mean value for this data), and negligible errors in all other parameters except u_*, then a $\pm 10\%$ error in u_* implies that z_{ch} can vary between 0.39 and 2.13 of the true value. Assuming the mean value of all the data is the true value, then one can plot the corresponding error bars for $\pm 10\%$ error in u_* as shown in Fig. 3. The corresponding error in c_p/u_* is approximately $\pm 9\%$.

It is noted from Fig. 3 that most of the data points lie within the $\pm 10\%$ error band for u_*. In other words, the apparent trend in the data is contained within the error band. In this situation, one cannot talk of a trend in the data. Rather, we will use the mean value of z_{ch} to characterize the dimensionless roughness from this set of measurements. Investigation into the individual field datasets presented in Fig. 2 of Donelan et al. (1993) indicates that for each dataset most of the points are contained within a $\pm 10\%$ error in u_* (see Figs. 4a–d). Now, since errors of $\pm 10\%$ in u_* are not unusual for conventional measurements, this indicates that it is difficult to infer trends from individual datasets.

Fortunately, the different datasets are collected in different wave age intervals. Hence, by using the mean values of z_{ch} corresponding to the mean value of wave age, one can plot all datasets together and infer a trend from the composite dataset. This plot is shown in Fig. 5 and it indicates a trend of decreasing z_{ch} with wave age. Note that in carrying out this composite analysis, we have assumed that all the datasets satisfy the four conditions described in section 4b above. A least squares fit of the composite data in Fig. 5 gives

$$z_{ch} = 1.89(c_p/u_*)^{-1.59}. \tag{4.19}$$

This expression is obtained in the wave age range $7 \le c_p/u_* \le 26$. Figure 6 shows a plot of all the data used in the analysis with the regression line [Eq. (4.19)]. It is seen that the regression line describes the general trend in the data reasonably.

Thus, it can be concluded that there is experimental evidence that the sea roughness depends on wave age. The next question is whether existing theories can be used to model this behavior. This question is examined in section 5. In section 4f, we discuss the question of self-correlation.

f. Problems with self-correlation in scaling with u_*

The question of spurious self correlation has been addressed by Smith et al. (1992). They obtained two conditions for negligible self-correlation in a relationship of the type: $z_{ch} = b(c_p/u_*)^a$. These conditions are

$$\mathrm{var}(\ln u_*^a) \ll \mathrm{var}(\ln z_{ch}) \tag{4.20}$$

$$\mathrm{var}(\ln u_*) \ll \mathrm{var}(\ln c_p), \tag{4.21}$$

where $\mathrm{var}(\cdot)$ is the variance of the variable within parentheses.

Using the logarithmic profile, $z_{ch} = (10g/u_*^2)\exp(-\kappa U_{10}/u_*)$, thus

$$\mathrm{var}(\ln z_{ch}) = \mathrm{var}(\ln u_*^2) + \mathrm{var}(-\kappa U_{10}/u_*), \tag{4.22}$$

where negligible covariance between $\ln u_*^2$ and U_{10}/u_* was assumed.

Now, Kahma and Calkoen (1994) obtained the following expression for fetch-limited wave growth in deep water:

$$\frac{\omega_p u_*}{g} = 3.08\left(\frac{gX}{u_*^2}\right)^{-0.27}, \tag{4.23}$$

where $\omega_p = 2\pi/T_p$ and X is the upwind fetch. Using Eq. (4.23), the wave celerity at peak frequency, c_p, is

$$c_p = \frac{u_*^{0.46} X^{0.27}}{3.08 g}. \tag{4.24}$$

Thus

$$\mathrm{var}(\ln c_p) = \mathrm{var}(\ln u_*^{0.46}) + \mathrm{var}(\ln X^{0.27}). \tag{4.25}$$

TABLE 1. Measured and derived data (wind direction = 270 ± 22.5, $u_* z_0/\nu > 2.3$).

Run name (YYMT-DDHHMM)	Depth (m)	H_{m0} (m)	T_p (sec)	U_7 (m s^{-1})	dir_{20} (deg)	$\langle uw \rangle$	$\langle vw \rangle$	z/L	u_* (m s^{-1})	C_p (m s^{-1})	U_{10n} (m s^{-1})	z_0 (m)	$1000C_{dn}$
9410060456	3.71	0.187	2.10	4.09	249	−0.0281	−0.0103	0.0742	0.17	3.25	4.14	0.00069	1.7432
9410110409	3.89	0.218	2.13	3.79	261	−0.0227	−0.0115	−0.1921	0.16	3.29	4.17	0.00029	1.4652
9410301114	3.93	0.222	2.28	6.40	256	−0.0619	−0.0098	−0.0321	0.25	3.51	6.80	0.00019	1.3535
9410141040	3.71	0.270	2.66	4.50	261	−0.0292	−0.0173	−0.1114	0.18	3.99	4.88	0.00025	1.4270
9410150822	3.97	0.274	2.52	5.46	269	−0.0474	−0.0128	−0.2078	0.22	3.84	6.01	0.00020	1.3604
9410150852	4.00	0.275	2.50	5.17	274	−0.0533	−0.0078	−0.1667	0.23	3.81	5.68	0.00056	1.6712
9410151122	3.99	0.279	2.65	5.04	286	−0.0479	−0.0174	−0.0848	0.23	4.00	5.44	0.00065	1.7191
9410171526	3.72	0.291	2.42	5.79	277	−0.0507	−0.0582	−0.0769	0.28	3.69	6.25	0.00123	1.9735
9410151052	4.02	0.291	2.75	4.50	286	−0.0306	−0.0179	−0.2360	0.19	4.13	4.98	0.00026	1.4313
9410140246	3.65	0.299	2.72	4.18	269	−0.0274	−0.0198	−0.2462	0.18	4.05	4.64	0.00041	1.5697
9410171556	3.71	0.309	2.52	5.06	291	−0.0417	−0.0145	−0.0894	0.21	3.82	5.46	0.00031	1.4801
9410150922	4.03	0.309	2.67	5.55	285	−0.0579	−0.0219	−0.1079	0.25	4.03	6.03	0.00062	1.7042
9411021111	3.94	0.324	2.88	4.96	285	−0.0414	−0.0088	0.0328	0.21	4.27	5.14	0.00046	1.6051
9410120222	3.60	0.341	2.74	6.05	257	−0.0507	−0.0165	−0.0215	0.23	4.07	6.41	0.00015	1.2970
9410131816	3.81	0.347	2.72	5.59	251	−0.0359	−0.0297	0.0233	0.22	4.07	5.82	0.00021	1.3758
9411020831	3.72	0.393	2.91	6.87	266	−0.0722	−0.0035	−0.0305	0.27	4.27	7.30	0.00019	1.3560
9411020959	3.87	0.425	3.07	6.26	276	−0.0569	0.0003	−0.0181	0.24	4.46	6.63	0.00015	1.2956
9410130032	3.80	0.427	3.03	8.47	279	−0.1025	0.0058	−0.0633	0.32	4.40	9.07	0.00012	1.2474
9410041204	3.95	0.441	3.14	8.53	262	−0.1061	−0.0167	−0.1201	0.33	4.55	9.24	0.00013	1.2575
9410041834	3.62	0.442	2.96	9.18	276	−0.1369	−0.0605	−0.0921	0.39	4.30	9.92	0.00035	1.5216
9410041404	3.83	0.450	2.91	10.42	282	−0.1747	−0.1055	−0.0951	0.45	4.29	11.27	0.00046	1.6058
9410041604	3.62	0.452	2.86	10.13	275	−0.1304	−0.0794	−0.1376	0.39	4.20	11.01	0.00013	1.2596
9410030700	3.44	0.456	2.84	9.93	259	−0.0777	−0.2107	−0.0061	0.47	4.15	10.48	0.00144	2.0457
9410130102	3.75	0.459	3.03	8.47	282	−0.0997	−0.0058	−0.0570	0.32	4.40	9.06	0.00011	1.2175
9410041704	3.58	0.462	3.04	8.81	265	−0.1076	−0.0382	−0.1067	0.34	4.37	9.52	0.00013	1.2593
9410041734	3.57	0.464	2.99	9.14	271	−0.1267	−0.0495	−0.1148	0.37	4.33	9.91	0.00022	1.3857
9410041634	3.59	0.483	3.04	9.56	281	−0.1406	−0.0723	−0.0950	0.40	4.38	10.33	0.00031	1.4813
9410130302	3.68	0.483	3.17	8.20	289	−0.1151	−0.0075	−0.0365	0.34	4.51	8.74	0.00034	1.5117
9410040849	3.92	0.487	3.31	8.37	272	−0.1143	−0.0335	−0.1196	0.35	4.69	9.09	0.00027	1.4424
9410041134	3.97	0.492	3.26	8.68	267	−0.1130	−0.0291	−0.1363	0.34	4.66	9.44	0.00016	1.3101
9410041019	3.98	0.492	3.29	9.03	265	−0.1246	−0.0392	−0.1316	0.36	4.69	9.82	0.00019	1.3558
9410041804	3.59	0.493	3.11	9.98	263	−0.1743	−0.0796	−0.0850	0.44	4.44	10.78	0.00053	1.6500
9410010234	3.37	0.496	2.90	12.50	248	−0.2128	−0.0506	−0.0154	0.47	4.20	13.22	0.00012	1.2514
9411012231	3.59	0.496	3.13	10.50	262	−0.1561	−0.0433	−0.0155	0.40	4.46	11.11	0.00016	1.3131
9410050504	3.50	0.503	3.10	9.20	284	−0.1158	−0.0352	−0.1326	0.35	4.41	9.98	0.00010	1.2141
9411020001	3.60	0.504	3.25	10.03	268	−0.1606	−0.0156	−0.0205	0.40	4.56	10.63	0.00025	1.4281
9410041934	3.70	0.504	3.05	8.90	283	−0.1192	−0.0189	−0.1271	0.35	4.41	9.66	0.00015	1.2936
9411012201	3.59	0.507	3.07	10.89	262	−0.1848	−0.0563	−0.0108	0.44	4.41	11.50	0.00028	1.4596
9410040719	3.82	0.510	3.34	9.40	279	−0.1288	−0.0266	−0.1562	0.36	4.70	9.87	0.00019	1.3509
9411012331	3.60	0.515	3.09	10.40	263	−0.1606	−0.0437	−0.0186	0.41	4.42	11.01	0.00020	1.3721
9410040749	3.85	0.515	3.33	8.68	275	−0.1213	−0.0487	−0.1381	0.36	4.69	9.46	0.00029	1.4611
9411012031	3.55	0.521	3.10	11.41	261	−0.1683	−0.0510	−0.0103	0.42	4.42	12.05	0.00010	1.2116
9411012301	3.59	0.523	3.29	10.74	264	−0.1662	−0.0478	−0.0133	0.42	4.60	11.35	0.00018	1.3416
9410040919	3.95	0.524	3.31	8.15	276	−0.0893	−0.0765	−0.1420	0.34	4.70	8.89	0.00031	1.4879
9410050404	3.53	0.526	3.33	9.77	280	−0.1313	−0.0431	−0.1214	0.37	4.61	10.58	0.00011	1.2334
9410010304	3.35	0.527	3.16	11.74	257	−0.1942	−0.0658	−0.0213	0.45	4.42	12.44	0.00017	1.3246
9411012131	3.58	0.528	3.17	10.39	260	−0.1415	−0.0370	−0.0121	0.38	4.49	10.98	0.00010	1.2138
9410042004	3.77	0.528	3.13	8.86	280	−0.1152	−0.0427	−0.1394	0.35	4.50	9.64	0.00017	1.3222
9410042234	3.88	0.528	3.36	9.15	276	−0.1385	−0.0689	−0.1064	0.39	4.73	9.92	0.00042	1.5718
9410050604	3.51	0.530	3.28	8.86	289	−0.1162	0.0012	−0.1535	0.34	4.57	9.65	0.00012	1.2473
9411012001	3.52	0.534	3.07	11.74	257	−0.2052	−0.0583	−0.0078	0.46	4.39	12.39	0.00022	1.3899
9411012101	3.57	0.537	3.31	11.21	261	−0.1689	−0.0567	−0.0132	0.42	4.60	11.85	0.00013	1.2690
9410050634	3.53	0.547	3.27	8.81	290	−0.1147	0.0118	−0.1517	0.34	4.56	9.60	0.00012	1.2522
9410042204	3.86	0.548	3.26	8.97	272	−0.1050	−0.0869	−0.0848	0.37	4.64	9.67	0.00028	1.4576
9410042134	3.84	0.552	3.26	8.73	273	−0.1106	−0.0512	−0.1089	0.35	4.63	9.45	0.00020	1.3647
9410040507	3.74	0.554	3.44	9.27	290	−0.1216	−0.0143	−0.1273	0.35	4.76	10.05	0.00010	1.2120
9410040949	3.96	0.559	3.48	8.86	264	−0.1412	−0.0562	−0.0873	0.39	4.85	9.57	0.00054	1.6584
9410042104	3.82	0.560	3.27	9.47	277	−0.1382	−0.0389	−0.1074	0.38	4.64	10.25	0.00020	1.3669
9411011931	3.47	0.561	3.12	12.06	253	−0.2312	−0.0497	−0.0056	0.49	4.42	12.72	0.00029	1.4622
9410050034	3.81	0.569	3.55	10.04	281	−0.1425	−0.0302	−0.1099	0.38	4.86	10.86	0.00011	1.2361
9411011901	3.44	0.570	3.13	12.95	253	−0.2631	−0.0745	−0.0154	0.52	4.42	13.70	0.00028	1.4564
9410041434	3.75	0.579	3.25	8.92	269	−0.1509	−0.0674	−0.0308	0.41	4.60	9.50	0.00088	1.8328
9410050104	3.78	0.586	3.57	10.38	278	−0.1530	−0.0662	−0.1054	0.41	4.86	11.22	0.00017	1.3233

TABLE 1. (*Continued*).

Run name (YYMT-DDHHMM)	Depth (m)	H_{m0} (m)	T_p (sec)	U_7 (m s^{-1})	dir_{20} (deg)	$\langle uw \rangle$	$\langle vw \rangle$	z/L	u_* (m s^{-1})	C_p (m s^{-1})	U_{10n} (m s^{-1})	z_0 (m)	$1000C_{dn}$
9410050004	3.83	0.586	3.40	9.77	277	−0.1479	−0.0314	−0.1109	0.39	4.75	10.58	0.00019	1.3511
9410042304	3.88	0.586	3.35	10.02	283	−0.1332	−0.0377	−0.1108	0.37	4.72	10.83	0.00009	1.1806
9410040607	3.76	0.589	3.49	8.60	286	−0.1069	−0.0183	−0.1315	0.33	4.80	9.33	0.00012	1.2446
9410050726	3.58	0.592	3.44	9.02	292	−0.1266	0.0092	−0.1362	0.36	4.71	9.81	0.00017	1.3195
9410040637	3.78	0.597	3.51	8.83	286	−0.1146	−0.0292	−0.1262	0.34	4.82	9.58	0.00014	1.2883
9411011301	3.65	0.603	3.32	13.62	248	−0.3233	−0.0930	−0.0022	0.58	4.63	14.35	0.00051	1.6348
9411011801	3.40	0.610	3.21	14.32	248	−0.4028	−0.1119	−0.0113	0.65	4.48	15.14	0.00086	1.8243
9411011831	3.43	0.622	3.23	14.07	253	−0.3394	−0.0883	−0.0150	0.59	4.50	14.89	0.00043	1.5820
9411011631	3.42	0.632	3.23	14.90	249	−0.3978	−0.1348	−0.0112	0.65	4.50	15.75	0.00060	1.6936
9411011331	3.59	0.634	3.23	14.30	248	−0.3523	−0.0950	−0.0046	0.60	4.54	15.08	0.00046	1.6056
9411011601	3.42	0.636	3.24	14.33	248	−0.3868	−0.1067	−0.0105	0.63	4.51	15.14	0.00070	1.7499
9411011701	3.41	0.640	3.19	14.28	248	−0.3742	−0.0923	−0.0144	0.62	4.46	15.11	0.00059	1.6880
9410031752	3.69	0.666	3.87	9.53	287	−0.1322	−0.0530	−0.1676	0.38	5.03	10.42	0.00016	1.3129
9411011431	3.52	0.672	3.33	15.49	248	−0.4602	−0.1237	−0.0079	0.69	4.61	16.35	0.00077	1.7821
9411011401	3.56	0.675	3.42	15.44	248	−0.4512	−0.1463	−0.0092	0.69	4.69	16.31	0.00077	1.7835
9411011501	3.48	0.691	3.29	15.05	248	−0.4537	−0.1422	−0.0077	0.69	4.57	15.89	0.00099	1.8835
9410031822	3.70	0.711	3.62	12.57	291	−0.2584	−0.0493	−0.0962	0.51	4.87	13.58	0.00025	1.4263

Using Eqs. (4.22) and (4.25) and the identity, $\text{var}(cY) = c^2\,\text{var}(Y)$ (where c is a constant and Y is a random variable), Eqs. (4.20) and (4.21) can be simplified to

$$a^2 \ll 4 + \frac{\text{var}(-\kappa U_{10}/u_*)}{\text{var}(\ln u_*)} \tag{4.26}$$

$$1 \ll 0.212 + 0.073\frac{\text{var}(\ln X)}{\text{var}(\ln u_*)}. \tag{4.27}$$

In general, Eq. (4.26) is satisfied if $|a| < 2$ (which is usually the case), while Eq. (4.27) is not necessarily satisfied. In fact, for a given site where the fetch varies slowly Eq. (4.27) will not be satisfied. Thus, self-correlation has some influence on results from a single site, as was found by Smith et al. (1992) for the HEXOS measurements. However, if the results from several sites with different fetches are aggregated together as done in this paper, $\text{var}(\ln X)$ is no longer close to zero, making it possible that Eq. (4.27) is satisfied. In this case, the influence of self-correlation due to scaling with u_* is significantly reduced. This provides an additional reason

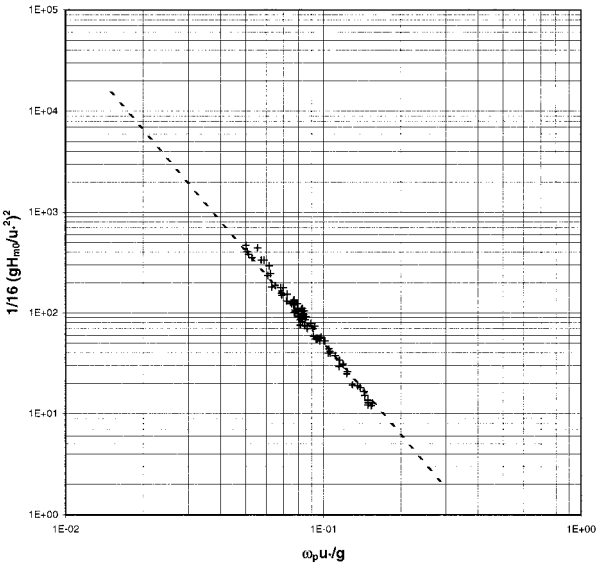

FIG. 2. Illustration of correlation between the dimensionless energy and peak frequency. The crosses represent the data, while the dotted lines is the relationship suggested by Toba (1978).

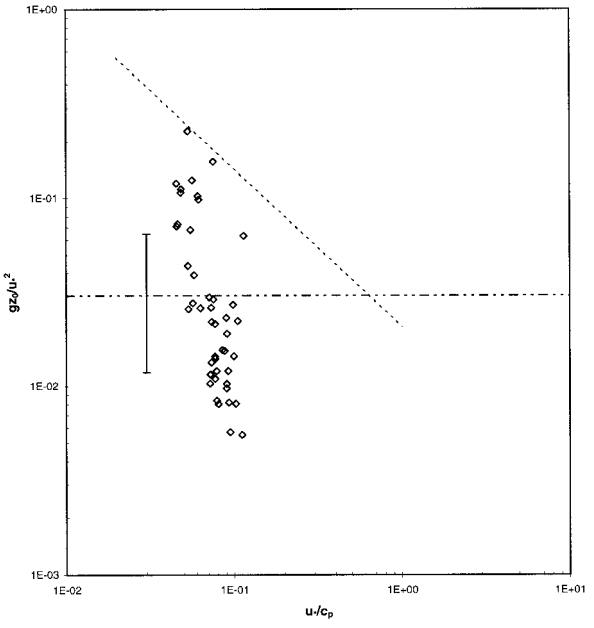

FIG. 3. Scatterplot of the Charnock parameter and inverse wave age for the RASEX dataset (diamonds). The dashed line is the relationship suggested by Toba et al. (1990), while the dash–dot line is the mean value for the Charnock parameter.

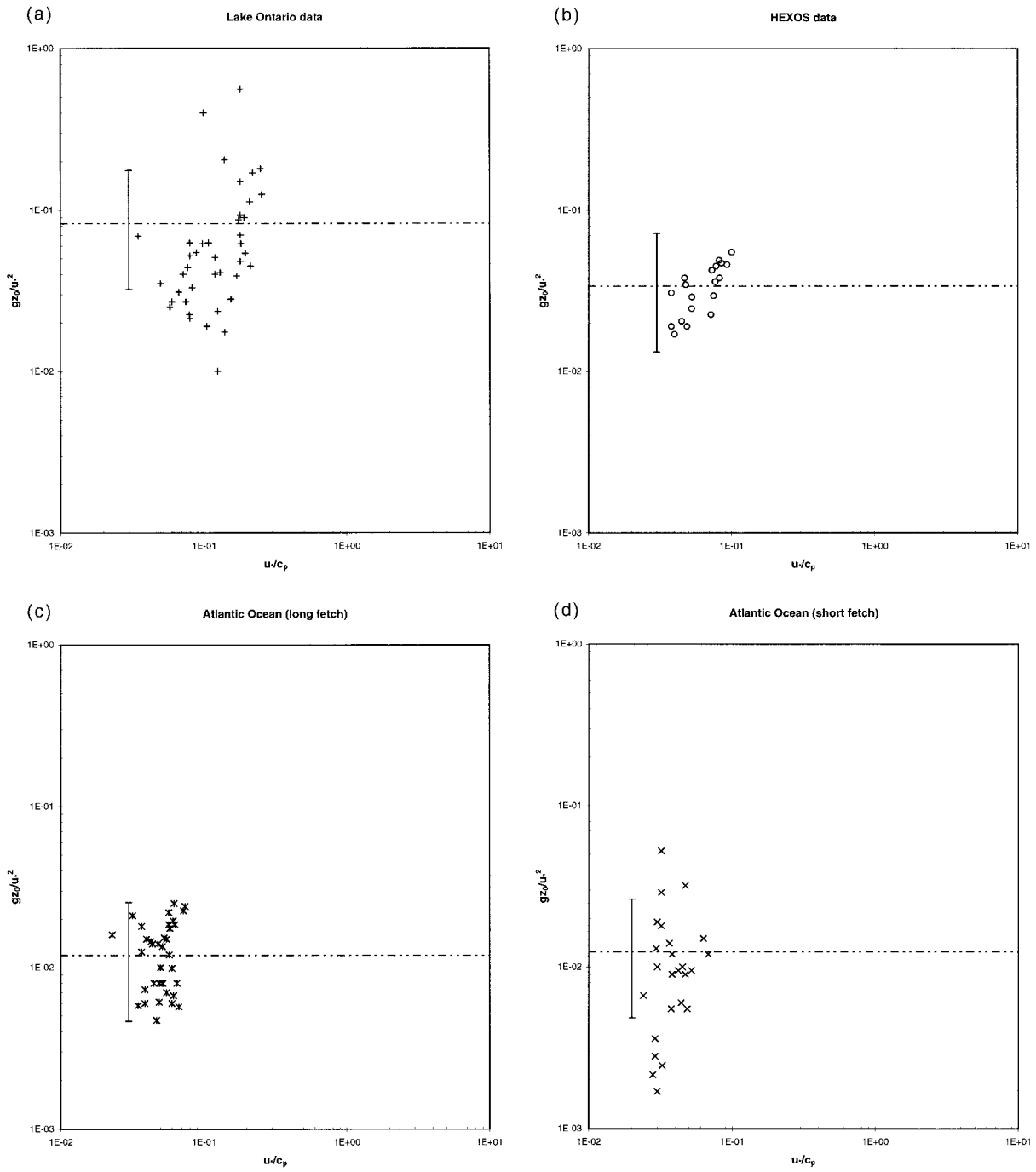

FIG. 4. Scatterplot of the Charnock parameter and inverse wave age for datasets compiled in Donelan et al. (1993). The dash–dot line is the mean value for the Charnock parameter.

why care must be taken in analyzing data from a single site.

5. Comparison with other roughness models

Below we discuss the comparisons between the measured stress values from the dataset and results derived from two different descriptions of the sea roughness, the one being Charnock expression, as depicted by Eq. (4.8). The second expression was derived by Hansen and Larsen (1997), who obtained an expression for the sea surface roughness by considering the waves as roughness elements in the sense of Lettau (1969), and combining this with Kitaigorodskii's idea about the in-

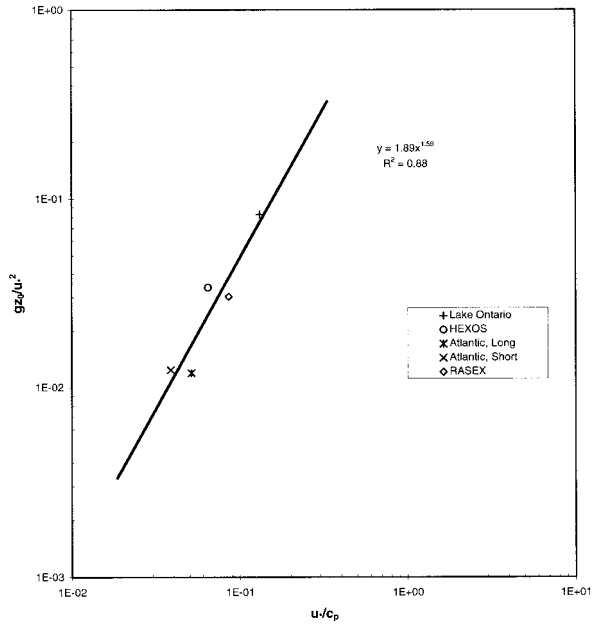

FIG. 5. Scatterplot of the mean Charnock parameter from different datasets and inverse wave age. The full line is the least squares best fit line.

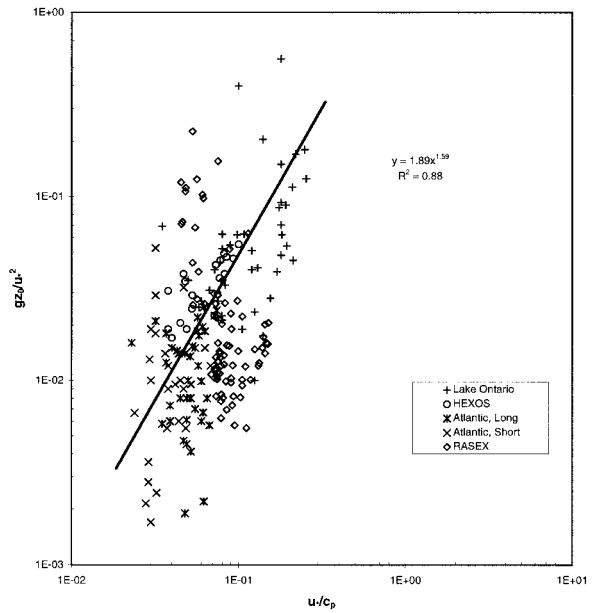

FIG. 6. Scatterplot of the Charnock parameter from different datasets and inverse wave age. The full line is the least squares best fit line from Fig. 4.4.

dividual roughness elements being wavelets moving with their individual phase speeds.

Kitaigorodskii (1970) noticed that the wavelets, considered as roughness elements, moved with their phase speed c relative to a stationary coordinate system. Since the wind profile in this system and any other inertial coordinate system moving with c should be given by the same logarithmic profile, the relation between the roughness effect of the wavelet in the stationary system z_0, and in the moving coordinate system z_c, should be given by

$$z_0 = z_c \exp(-\kappa c/u_*), \tag{5.1}$$

where z_0 is the roughness experienced by the wind, while z_c is the corresponding roughness in a coordinate system moving with the phase speed of the wave c, κ is the von Kármán constant, and u_* is the friction velocity.

The value for z_c for a field of roughness elements is estimated from Lettau's (1969) relation for roughness elements:

$$z_c = \alpha_L hX/A, \tag{5.2}$$

where α_L is a coefficient of order unity, h is the height of the element, X its cross-wind area, and A is the horizontal area available to each element. Identifying h in Eq. (5.2) with the wave height (twice the amplitude a) and X/A with ak/π (where k is the wavenumber), Hansen and Larsen transform Eq. (5.2) to a form appropriate for wavelets:

$$z_c = \begin{cases} \alpha_L hX/A = \dfrac{2}{\pi}\alpha_L a^2 k = \dfrac{2}{\pi}\alpha_L s^2 k^{-1}, \\ \qquad s > s_0 \qquad\qquad (5.3a) \\ 0 \\ \qquad s \le s_0. \qquad\qquad (5.3b) \end{cases}$$

In Eq. (5.3), it is implied that only wavelets with a steepness, s ($s = ak$), larger than s_0 can create flow separation and thereby qualify as roughness elements. The value of s_0 is found to be between 0.25 and 0.3.

To interpret Eq. (5.3) it is assumed that the roughness wavelets constitute a random superposition of harmonic components in a narrow wavenumber band, that is, essentially of one wavenumber, $\langle k\rangle$, defined by

$$\langle\eta^2\rangle\langle k\rangle = \int_k^\infty k'F(k')k'\,dk' \tag{5.4}$$

$$\langle\eta^2\rangle = \int_k^\infty k'F(k')k'\,dk' = \int_\omega^\infty S(\omega')\,d\omega', \tag{5.5}$$

where $F(k)$ is the one-dimensional wavenumber spectrum of the surface displacement $\eta(x, t)$ and $S(\omega)$ is the omnidirectional frequency spectrum.

To derive the average $\langle z_c\rangle$ from a given $\langle k\rangle$, Hansen and Larsen (1997) argue that the steepness s in Eq. (5.3) essentially follows an exponential distribution in the normalized variable, $y = s^2/(2\langle\eta^2\rangle\langle k\rangle^2)$. Using this exponential distribution and averaging z_c over all steepness values larger than s_0, the average contribution to z_c, $\langle z_c\rangle$, from a narrow k interval around $\langle k\rangle$ was found as function of $\langle k\rangle$.

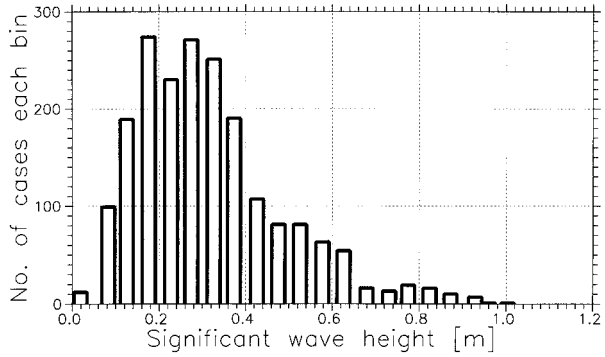

FIG. 7. Distribution of significant wave heights for the RASEX dataset.

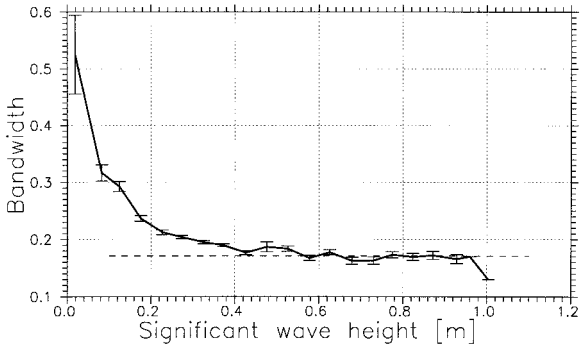

FIG. 8. Bandwidth of RASEX wave spectra.

$$\langle z_c \rangle = \alpha_L \frac{2}{\pi} \langle \eta^2 \rangle x e^{-x} \langle k \rangle, \tag{5.6}$$

where x is the normalized critical steepness:

$$x = \frac{s_0^2}{2\langle \eta^2 \rangle \langle k \rangle^2}. \tag{5.7}$$

The contribution to $\langle z_c \rangle$ from an infinitesimal wavenumber interval dk is found by differentiating $\langle \eta^2 \rangle \langle k \rangle$ in Eq. (5.6) using Eq. (5.4) to yield

$$d\langle z_c \rangle = \alpha_L \frac{2}{\pi} x e^{-x} k F(k) k \, dk. \tag{5.8}$$

Equation (5.8) is finally combined with Eq. (5.1) to yield the contribution to z_0 from and infinitesimal wavenumber interval dk:

$$dz_0 = \alpha_L \frac{2}{\pi g} x e^{-x} e^{-\kappa g/\langle \omega \rangle u_*} \omega^2 S(\omega) \, d\omega, \tag{5.9}$$

where x and $\langle \omega \rangle$ are to be evaluated by use of Eqs. (5.4) and (5.5) with $\omega^2 = gk$, when needed.

Subsequently integrating over ω, using the Kitaigorodskii form of $S(\omega)$, Hansen et al. (1990) and Hansen and Larsen (1997) find the contribution to z_0 from different frequencies for different sea states. The behavior is similar, but not identical, to that of the Kitaigorodskii model (Kitaigorodskii and Volkov 1965; Kitaigorodskii 1970) and has the advantage that the empirical coefficient, α_L, in Eq. (5.9) is of order unity as opposed to the other models available for the sea roughness.

a. From wave spectrum to roughness length

The derivation of roughness lengths from the measured wave spectra is quite time consuming and somewhat complicated because of the integration involved in the calculation of Eq. (5.9). Instead, we have chosen a simpler method in which a model wave spectrum is fitted to the data using only measured values of peak frequency f_p and the measured significant wave height H_s. The computations can then be greatly simplified by tabulating the spectral moments of the waves and doing the integrations at a certain number of fixed frequencies. The necessary steps from measurements to resulting roughness lengths are then

1) Find a suitable spectral model that fits the data sufficiently well.
2) Screen the data to exclude unwanted wind directions, situations with ''strange'' spectra and low wind speeds with large measurement errors.
3) Compute roughness lengths from spectral model.
4) Compare wind stress derived from roughness lengths of ''3'' and mean wind speed (log-windprofile) with directly measured windstress.
5) If there are systematic differences in ''4,'' then go back to ''3,'' multiply the roughness lengths with a constant and check differences again.

b. Model wave spectrum

The model chosen is a JONSWAP-type spectrum (Hasselmann et al. 1973):

$$S(f) = \alpha_P g^2 (2\pi)^{-4} f^{-5} \exp\left[-\frac{5}{4} \left(\frac{f}{f_p} \right)^{-4} \right] \gamma^{\Gamma}, \tag{5.10}$$

where

$$\Gamma = \exp\left(-\frac{(f - f_p)^2}{2\sigma^2 f_p^2} \right),$$

where α_P is the Phillips constant, g is acceleration of gravity (m s^{-1}), f is frequency (Hz), f_p is peak frequency, γ is peak enhancement factor, and σ is 0.07 for $f < f_p$, 0.09 for $f > f_p$.

We used the somewhat simplified version of Eq. (5.10) with $\gamma = 1.0$. As shown below the simplified model fits the data well.

The distribution of available time series as a function of wave height is shown in Fig. 7. To check the applicability of the model we compared measured spectral bandwidths to model bandwidth (Fig. 8). We see that for a wide range of wave heights we get good correspondence between model and data. As expected, the waves with small amplitudes also show spectra that are

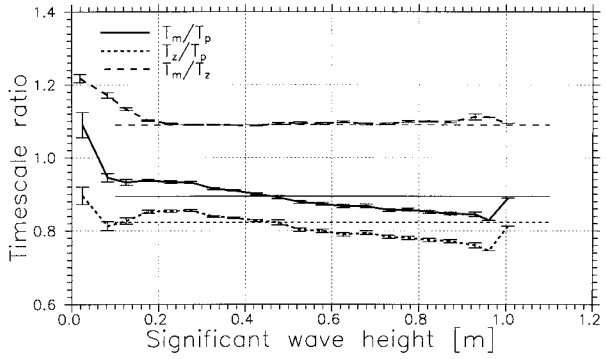

FIG. 9. Comparison between ratios of measured characteristic wave periods and model derived wave periods. Model values are shown as horizontal lines.

wider than the model; in some cases clear two-peaked behavior was seen. The measured wave periods are compared with the model parameters in Fig. 9, from which we can see that there seems to be some systematic change of the peak shape with T_p increasing slightly for increasing wave height compared to the model, whereas the periods based on the spectral moments (dominated by higher frequencies) are very well modeled.

c. Screening of data

The data used in the analysis here were screened according to the following criteria:

- Wind direction: Only directions with an undisturbed fetch of 10–20 km were used (the longest usable fetch from the RASEX experiment), that is, 240°–330°.
- Wave spectra: Only data with spectra with a bandwidth BW $<$ 0.3 were used.
- Wind stress: Only data with measured stress >0.0025 m^2 s^{-2} (friction velocity $u_* > 0.05$ m s^{-1}) were used.
- Wind speed: Because of the sampling method applied, the mean wind speeds measured by the cup anemometers were unreliable for speeds <2 m s^{-1}, which were then excluded.
- Wave height: Significant wave heights <0.1 m were excluded.
- Roughness: Roughness lengths computed from the wave spectra with values $z_0 < 10^{-10}$ m were not used.

After screening for spectral widths, wind stress, wave height, and roughness about 1500 datasets remained. Selecting the proper wind direction sector left us with 576 30-min time series that were used.

d. Wind stress

The friction velocities were computed from the roughness lengths inferred from the wave spectra using

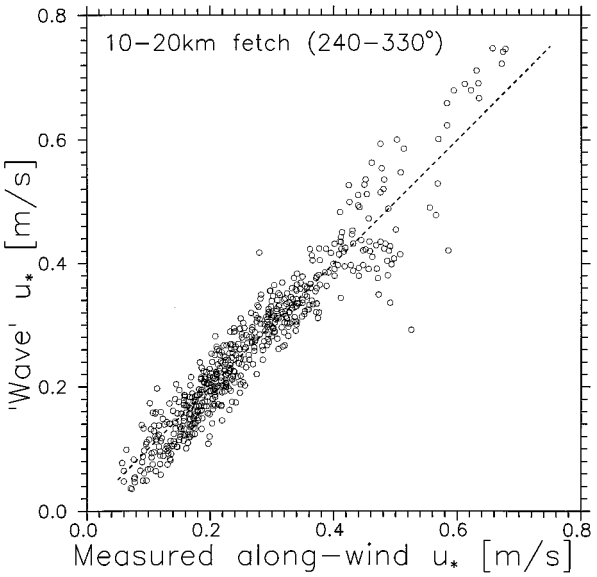

FIG. 10. Comparison between measured u_* ($=-|\langle uw\rangle|^{0.5}$) and u_* derived from the log wind profile and z_0 from the wave spectra.

Eq. (5.9), the mean wind speed at a height of 7 m in the logarithmic profile. The computed friction velocities were compared with the alongwind component of the wind stress measured at 3 m, that is, $u_*^2 = \langle -u'w'\rangle$. A least squares fit was calculated and the roughness lengths were multiplied by a constant in order to obtain a 1:1 relation between the measured and calculated values. The value of the constant that was used was 5.0. The fit was forced through 0. The results are shown in Fig. 10, from which we can see that the correspondence is very good with the spreading somewhat increasing at friction velocities higher than 0.4 m s^{-1}.

We can also derive the friction velocity from the Charnock relation

$$z_0 = A\frac{u_*^2}{g}, \tag{5.11}$$

where we can use the logarithmic wind profile to derive an implicit equation for u_*, that can easily be iterated using a measured value of the wind speed U.

$$z\exp\left(-\frac{U\kappa}{u_*}\right) = A\frac{u_*^2}{g}, \tag{5.12}$$

where z is the height above the surface, U the mean wind speed, and κ the von Kármán constant ($=0.4$).

The resulting friction velocities were compared with the measured friction velocities and the calculated values were adjusted to a 1:1 relationship by adjusting the Charnock constant A to a value of 0.018 (see Fig. 11), which as expected for this coastal site is on the high side of the range found in the literature, $0.011 < A < 0.018$ (among others, Wu 1980; Garratt 1977; Smith and Banke 1975; Walmsley 1988).

Finally, in Fig. 12 we have compared the bin-aver-

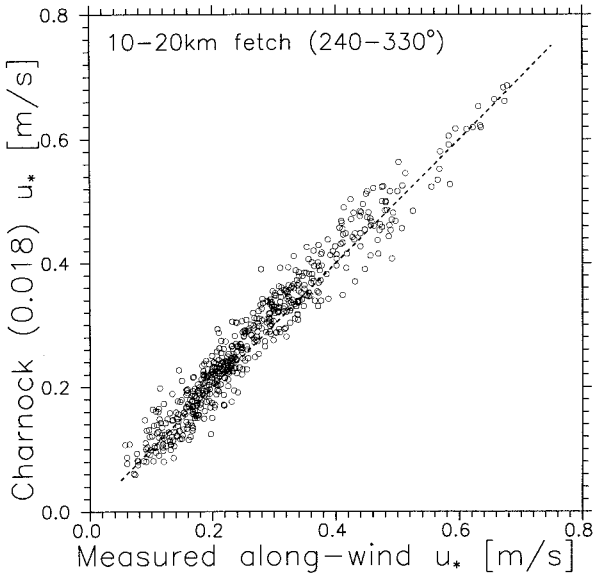

FIG. 11. Comparison between measured friction velocity and the friction velocity derived using the Charnock relation with a Charnock constant of 0.018.

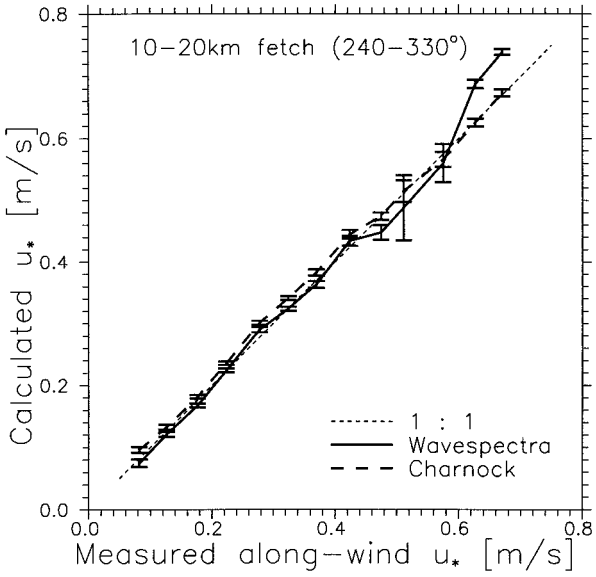

FIG. 12. Binned averages of the data from Figs. 10 and 11. The vertical bars signify ±1 standard error on the mean value.

aged values of the two different estimates of friction velocities, and we can see that the Hansen and Larsen method gives rise to slightly larger variations, and some deviations from the straight line above 0.4 m s^{-1}. The Charnock u_* shows small deviations from the straight line at small friction velocities (the least squares fit showed an offset of 0.01 m s^{-1}.

e. The Charnock "constant"

The variation of the Charnock constant A in Eq. (5.11) is plotted in Fig. 13 as a function of inverse wave age. Here we have used the z_0 values calculated from the wave spectra and the directly measured u_*. Furthermore, the data have been subdivided into classes of different flow regimes using the method of Kraus and Businger (1994):

Aerodynamically smooth flow: $u_* < 0.11$ m s^{-1}
Transition flow: 0.11 m s^{-1} $< u_* <$ 0.265 m s^{-1}
Fully rough flow: 0.265 m s^{-1} $< u_*$.

This classification is based on a roughness Reynolds number ($u_* z_0/\nu$) in which z_0 is replaced by the Charnock value. Obviously smooth flow is most often found in cases with old waves and rough flow in situations with younger, developing waves. We observe a systematic variation of gz_0/u_*^2 with increasing values for decreasing wave age as discussed in section 4.

If instead of using the z_0 values derived using Hansen and Larsen we use the z_0 values from the Chamock relation, we see a quite different relation as seen in Fig. 14. This figure shows how well u_*^2 is predicted using the Charnock relation, since gz_0/u_*^2 is the same as $z_{ch}u_{*,\text{Charnock}}^2/u_{*,\text{measured}}^2$. Here, we see a systematic overprediction of u_*^2 for the old waves (low inverse wave age). For the younger waves (and fully rough flow), this overprediction is diminished, since the mean trend tends toward 0.018 (the value for z_{ch}).

When we are only interested in predicting the wind stress, then we seem to get slightly better results by using a simple Charnock relation, at least for a relatively narrow range of wave ages. On the other hand, we know from the aggregation of experimental results from different sites (Fig. 5) that there seems to be a strong in-

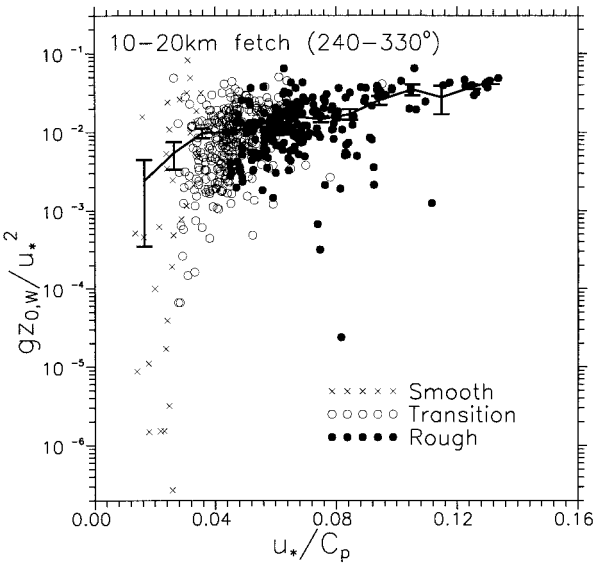

FIG. 13. Charnock constant plotted as a function of inverse wave age. The z_0 values were derived from the wave spectra.

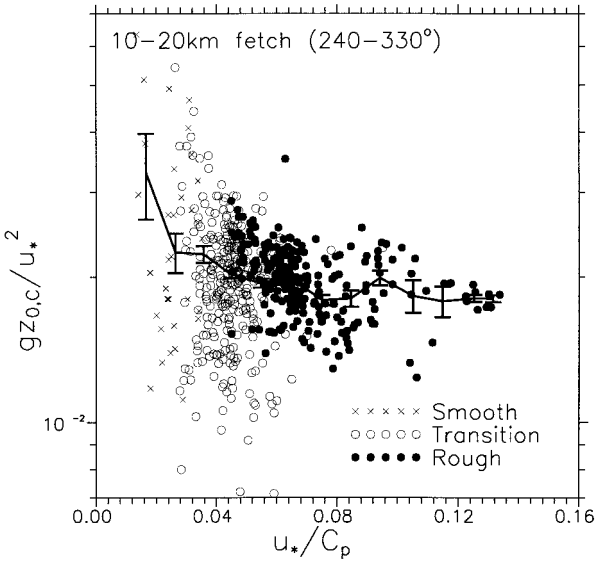

FIG. 14. As in Fig. 13 only here z_0 was derived from the Charnock relation.

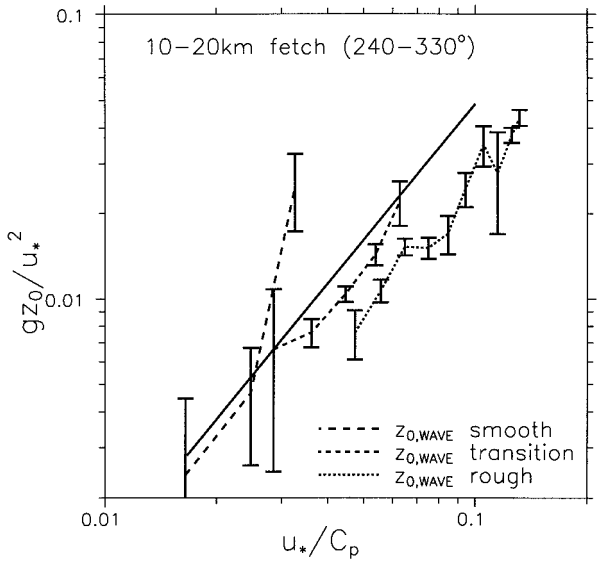

FIG. 15. Bin-averaged values from Fig. 5.7 with $z_{0,WAVE}$ values subdivided into different flow regimes. The vertical bars signify ± 1 standard error on the mean. The thick line is Eq. (4.19).

crease of gz_0/u_*^2 with decreasing wave age over a wide range of wave ages, which is quite nicely reproduced by the Hansen and Larsen method. Hence, the Charnock method is good for a limited range of wave ages if you can guess the value of the Charnock constant, but the spectral method seems to give a more correct picture in the sense that it is capable of reproducing the variation of the Charnock constant with wave age.

Finally, in Fig. 15, we have overlaid the binned results from the Charnock method with the results from the Hansen and Larsen method, where the latter has been subdivided into three different flow regimes. It seems that the average of the curve for the rough flow is consistent with the Charnock results. Furthermore, the Hansen and Larsen method qualitatively reproduce the trend of the Charnock parameter obtained from aggregating various field datasets.

Further investigations on the use of existing theories for air–sea momentum flux and implications for wave modeling at the RASEX site was made using WAM cycle 4 model (see Johnson et al. 1997, submitted to *J. Oceanic Atmos. Technol.*). In that paper, the use of Janssen's theory in the WAM model, and its applicability at the RASEX site, is discussed at length.

6. Summary and conclusions

1) Dimensionless analysis of the air–sea interaction problem yields a relationship between the dimensionless sea roughness and wave age under specific conditions.
2) Using a selected dataset from RASEX satisfying the conditions in (1), a weak trend of increasing dimensionless roughness with wave age was observed. However, error analysis indicates that measurement errors of about 10% in u_* makes it difficult to conclude on the trend in z_{ch} using measured data from a particular dataset. This conclusion was found to be equally valid for other field datasets compiled in Donelan et al. (1993). It was also found that self-correlation plays a role in the trend observed from data from a single site.
3) Analysis of the mean dimensionless sea roughness (Charnock parameter) from the field datasets mentioned in 2) gives a trend of decreasing Charnock parameter with wave age. The fitted relationship is $z_{ch} = 1.89(C_p/U_*)^{-1.59}$. This relationship establishes the mean trend in the variation of dimensionless sea roughness with wave parameters under the conditions identified in 1) for field data.
4) The wave-dependent sea roughness expression of Hansen and Larsen (1997) was found to reproduce the measured friction velocities in RASEX quite well. Furthermore, it qualitatively reproduced the trend of the Charnock parameter obtained by combining many field datasets.
5) A constant Charnock parameter of 0.0180 was found to adequately reproduce measured friction velocities in the RASEX experiment.
6) From the above results, we conclude that there is evidence that a wave-age-dependent sea roughness is necessary to explain the variation of sea roughness over a wide range of wave ages. Thus, for large-scale models, a wave-age-dependent sea roughness models would be necessary. However, for a relatively small range of wave ages, typical of a given site (or a limited area study), a constant Charnock parameter

representative of the typical wave age at the site can be used. In this case, the Charnock parameter may be estimated (as a first guess) using Eq. (4.19). However, the need to guess the correct Charnock parameter for each site emphasises the need to use a wave-age-dependent formulation.

Acknowledgments. The research was funded by the Danish Technical Research Council (STVF) as part of the project ''Wind-wave interaction in coastal and shallow areas'' and the Commission of the European Communities, Directorate General for Science, Research and Development for the ECAWOM project. We gratefully acknowledge the financial support of the RASEX measurement campaign by the following: European Union, JOULE program (JOU2-CT93-0325), Office of Naval research (N00014-93-1-0360), and ELKRAFT. Furthermore, we thank members of the ECAWOM group, especially Dr. G. Komen, for their comments and suggestions. Thanks are also due to the reviewers for useful comments and suggestions.

REFERENCES

Barthelmie, R. J., M. S. Courtney, J. Højstrup, and P. Sanderhoff, 1994:The Vindeby Project: A description. Rep. Risø-R-741 (EN), Risø National Laboratory, Roskilde, Denmark.

Charnock, H., 1955: Wind stress on a water surface. *Quart. J. Roy. Meteor. Soc.,* **81,** 639–640.

Donelan, M. A., 1982: The dependence of the aerodynamic drag coefficient on wave parameters. *Proc. of the First Int. Conf. on Meteorology and Air/Sea Interaction of the Coastal Zone,* the Hague, the Netherlands, Amer. Meteor. Soc. 381–387.

——, 1990: Air–sea interaction. *The Sea,* B. LaMehaute and D. Hanes, Eds., Vol. 9, John Wiley and Sons, 239–292.

——, F. W. Dobson, S. D. Smith, and R. J. Anderson, 1993: On the dependence of sea surface roughness on wave development. *J. Phys. Oceanogr.*, **23,** 2143–2149.

Garratt, J. R., 1977: Review of drag coefficients over oceans and continents. *Mon. Wea. Rev.,* **105,** 915.

Geernaert, G. L., K. B. Katsaros, and K. Richter, 1986: Variation of the drag coefficient and its dependence on sea state. *J. Geophys. Res.*, **91,** 7667–7679.

——, S. E. Larsen, and F. Hansen, 1987: Measurements of the wind stress, heat flux and turbulence intensity during storm conditions over the North Sea. *J. Geophys. Res.,* **92** (C), 13 127–13 139.

Hansen, C., and S. E. Larsen, 1997: Further work on the Kitaigorodskii roughness length model: A new derivation using Lettau's expression on steep waves. *Geophysica,* **33** (2), 29–44.

——, K. B. Katsaros, S. A. Kitaigorodskii, and S. E. Larsen, 1990: The dissipation range of wind-wave spectra observed on a lake. *J. Phys. Oceanogr.,* **20,** 1264–1277.

Hasselmann, K., and Coauthors, 1973: Measurements of wind-wave growth and swell decay during JONSWAP. *Dtsch. Hydrogr. Z. A8* (Suppl), **12,** 95.

Kahma, K. K., and C. J. Calkoen, 1994: Growth curve observations. *Dynamics and Modelling of Ocean Waves,* G. L. Komen et al., Eds., Cambridge University Press, 174–182.

Keller, M. R., W. C. Keller, and W. J. Plant, 1992: A wavetank study of the dependence of X-band cross sections on wind speed and water temperature. *J. Geophys. Res.*, **97,** 5771–5792.

Kitaigorodskii, S. A., 1970: *The Physics of Air–Sea Interaction.* Israel Program for Scientific Translations, 273 pp.

——, and Y. A. Volkov, 1965: On the roughness parameter of the sea surface and the calculation of momentum flux in the lower layer of the atmosphere. *Izv. Atmos. Oceanic Phys.*, **4,** 498–502.

Kraus, E. B., and J. A. Businger 1994: *Atmosphere–Ocean Interaction.* Oxford University Press, 362 pp.

Lettau, H., 1969: Note on aerodynamic roughness-parameter estimation on basis of roughness element distribution. *J. Appl. Meteor.*, **8,** 820–832.

Maat, N., C. Kraan, and W. A. Oost, 1991: The roughness of wind waves. *Bound.-Layer Meteor.*, **54,** 89–103.

Merzi, N., and W. H. Graf, 1985: Evaluation of the drag coefficient considering the effects of mobility of the roughness elements. *Ann. Geophys.*, **3,** 473–478.

Phillips, D. M., 1977: *Dynamics of the Upper Ocean.* 2d ed. Cambridge University Press, 336 pp.

Smith, S. D., and E.G. Banke, 1975: Variation of the sea surface drag coefficient with wind speed. *Quart. J. Roy. Meteor. Soc.,* **101,** 665–673.

——, R. J. Anderson, W. A. Oost, C. Kraan, N. Maat, J. DeCosmo, K. B. Katsaros, K. L. Davidson, K. Bumke, L. Hasse, and H. M. Chadwick, 1992: Sea surface wind stress and drag coefficients: The HEXOS results. *Bound.-Layer Meteor.*, **60,** 109–142.

Toba, Y., 1978: Stochastic form of the growth of wind waves in a single parameter representation with physical implications. *J. Phys. Oceanogr.,* **8,** 494–507.

——, N. Lida, H. Kawamura, N. Ebuchi, and I. S. F. Jones, 1990: Wave dependence on sea-surface wind stress. *J. Phys. Oceanogr.,* **20,** 705–721.

Walmsley, J. L., 1988: On theoretical wind speed and temperature profiles over the sea with applications to data from Sable Island, Nova Scotia. *Atmos.–Oceans,* **26,** 203.

Wu, J., 1980: Wind stress coefficients over sea surface near neutral conditions. A revisit. *J. Phys. Oceanogr.,* **10,** 727–740.